Epitaxial-Strain-Induced Multiferroicity in SrMnO$_3$ from First Principles

Jun Hee Lee[*] and Karin M. Rabe

Department of Physics and Astronomy, Rutgers University, Piscataway, New Jersey 08854-8019, USA
(Received 27 October 2009; published 20 May 2010)

First-principles calculations reveal a large spin-phonon coupling in cubic SrMnO$_3$, with ferromagnetic ordering producing a polar instability. Through combination of this coupling with the strain-polarization coupling characteristic of perovskites, the bulk antiferromagnetic-paraelectric ground state is driven to a previously unreported multiferroic ferroelectric-ferromagnetic state by increasing epitaxial strain. This state has a computed $P_s > 54$ μC/cm^2 and magnetic $T_c > 92$ K. Large mixed magnetic-electric-elastic responses are predicted in the vicinity of the phase boundaries.

Multiferroic materials have been the subject of continuing attention both for fundamental physics and for potential applications including transducers and information storage [1–3]. There is particular interest in the search for multiferroic materials with large polarization ($P > 1$ μC/cm^2) and magnetization that persists to high temperatures, as well as a strong coupling between the magnetism and the electric polarization.

With epitaxial strain, it is possible to widen the search to include phases and phase boundaries that do not appear in bulk. In many paraelectric perovskite oxides, epitaxial strain couples strongly to the lowest-frequency polar phonon; this is responsible for the phenomenon of epitaxial-strain-induced ferroelectricity, which has been intensively studied both experimentally and theoretically [4–6]. In an antiferromagnetic-paraelectric system, there is a further intriguing possibility. If the system has a spin-phonon coupling in which the lowest-frequency polar phonon is softer for ferromagnetic ordering than for antiferromagnetic ordering, then epitaxial strain enhancement of a polar instability lead to the lowering of the energy of the ferromagnetic (FM)-ferroelectric (FE) state below that of the antiferromagnetic (AFM)-paraelectric (PE) state. This mechanism for producing a multiferroic phase was proposed and elucidated using first-principles calculations for EuTiO$_3$ [7]. Unfortunately, the Curie temperature is of the same scale as the bulk Néel temperature of 5.5 K [8], and thus the multiferroic phase is observed only at very low temperatures.

The demonstration of the spin-phonon coupling mechanism for epitaxial-strain-induced multiferroicity in EuTiO$_3$ suggests a search for other paraelectric antiferromagnetic materials in which this mechanism could be realized and the ferroic ordering temperatures increased. The primary criterion is that of a large downward shift in the frequency of the lowest polar phonon with ferromagnetic ordering, which leads to a large energy gain for polar distortion of the ferromagnetic state. In addition, we look for systems with a moderate Néel temperature (T_N): while it would be preferable to have the magnetic ordering temperatures as high as possible, this is limited by the fact that the FM-

AFM energy splitting cannot be larger than the scale of the energy gain for polar distortion of the ferromagnetic state. Finally, the polar instability should be strong enough to compete with any other structural distortions, such as oxygen octahedron rotations.

B-site magnetic perovskite oxides are of particular interest, as the larger exchange coupling results in much higher magnetic ordering temperatures than that of A-site rare-earth systems such as EuTiO$_3$. Perovskite manganites are especially promising as they show strong magneto-electronic and magnetostructural effects, including colossal magnetoresistance [9] and magnetic-field-induced structural transitions [10]. Indeed, a first-principles survey of the phonon dispersions of cubic perovskite oxides, including previously reported results on chromites [11] and our own investigations of chromites, ferrites, and manganites [12] shows strong spin-phonon coupling in both SrMnO$_3$ and CaMnO$_3$. Here, we discuss only SrMnO$_3$, which in bulk is observed to have a paraelectric cubic perovskites structure with G-type AFM ordering below $T_N = \sim 233$–260 K [13,14].

In this Letter, we report first-principles investigation of the strong spin-phonon coupling and resulting epitaxial-strain-induced multiferroic phases in SrMnO$_3$. Futhermore, we predict large mixed magnetic-electric-elastic responses in the vicinity of the phase boundaries. In comparison to EuTiO$_3$, the larger energy scales for magnetic ordering, structural distortions, and spin-phonon coupling correspond to an increase in the multiferroic critical temperature of well over an order of magnitude.

First-principles calculations were performed using density-functional theory within the generalized gradient approximation GGA $+ U$ method [15] with the Perdew-Becke-Erzenhof parametrization [16] as implemented in the Vienna *ab initio* simulation package (VASP-4.6) [17,18]; selected LSDA $+ U$ calculations were performed for comparison. We use the Dudarev [19] implementation with on-site Coulomb interaction $U = 2.7$ eV and on-site exchange interaction $J_H = 1$ eV to treat the localized d electron states in Mn. Within GGA $+ U$, this choice gives agreement between the calculated (2.7 μ_B) and experi-

mental magnetic moments (2.6 $\mu_B \pm 0.2$) [14] and is similar to that in a previous GGA + U study [20]. The projector augmented wave (PAW) potentials [21] explicitly include 10 valence electrons for Sr ($4s^2 4p^6 5s^2$), 13 for Mn ($3p^6 3d^5 4s^2$), and 6 for oxygen ($2s^2 2p^4$).

The phonon frequencies of the ideal cubic perovskite G-AFM and FM reference structures were computed using the frozen phonon method in a $\sqrt{2} \times \sqrt{2} \times 2$ supercell with a $6 \times 6 \times 4$ Monkhorst-Pack (M-P) k-point mesh at the Γ, R, X, and M points of the primitive perovskite Brillouin zone.

To find the minimum-energy configuration in a given space group determined by freezing in one or more unstable modes of the cubic reference structure, we moved the atoms according to the conjugate-gradient algorithm until the residual Hellman-Feynman forces were less than 1.0 meV/Å. Structural optimizations were performed for 20-atom $\sqrt{2} \times \sqrt{2} \times 2$ supercell with a $4 \times 4 \times 4$ M-P k-point mesh; for A-AFM $R_+^4[110] + \Gamma_4^-[110]$, a $2 \times 2 \times 2$ supercell with a $4 \times 4 \times 4$ M-P k-point mesh was used.

To study the effects of epitaxial strain, we performed "strained-bulk" calculations [22,23]. Epitaxial strain is here defined relative to the computed lattice constant for the G-AFM cubic perovskite structure (3.845 Å). Ferroelectric polarizations for the relaxed structures at each strain were computed by the Berry-phase method [24]. Curie and Néel temperatures for a given strain are estimated from the energy differences between FM and G, C and A-AFM orderings assuming two exchange constants (in-plane and out-of-plane nearest neighbor couplings) and applying mean field theory [25]. To obtain a prediction useful for quantitative comparison with experiment, we uniformly rescaled the temperatures so that the value for the bulk cubic perovskite phase $T_{N,MFT} = 277$ K corresponds to the experimental value of $T_N = 260$ K [14].

The calculated lattice constants of cubic G-AFM and FM SrMnO$_3$ are $a = 3.845$ Å and 3.865 Å, respectively; the slight overestimate relative to the experimental G-AFM value $a = 3.80$ Å [14] is typical of GGA calculations for oxides. The computed lowest phonon frequencies of cubic FM and G-AFM SrMnO$_3$ at the computed lattice constant for the cubic G-AFM structure are shown in Table I; for the cubic FM structure, the computed lattice constant is very similar and the effect of the difference on the phonon frequency, also is given in Table I, is small except at Γ.

Across the Brillouin zone, the FM modes are lower in frequency than the corresponding modes in the G-AFM

TABLE I. Calculated lowest phonon frequencies, in cm^{-1}, of cubic SrMnO$_3$ at calculated equilibrium lattice constants with G-AFM and FM orderings for high symmetry q points.

	Γ	X	R	M
G-AFM ($a_0 = 3.845$ Å)	121	116	84.5i	38.1i
FM ($a_0 = 3.845$ Å)	76.2i	116	114i	86.3i
FM ($a_0 = 3.865$ Å)	109i	113	119i	89.9i

structure. This effect is especially dramatic at Γ, where the lowest frequency TO mode is stable in the G-AFM structure but unstable in the FM structure. The corresponding eigenvectors are (Sr, Mn, O$_{||}$, O$_\perp$) = (0.10, 0.31, -0.52, -0.56) for G-AFM and (0.03, 0.41, -0.42, -0.57) for FM, showing displacement of both the Sr and Mn cations relative to a fairly rigid oxygen octahedral network.

From the presence of unstable modes, it is clear that the computed ground state of SrMnO$_3$ is not the ideal cubic perovskite structure. However, the energy gains and distortions for the G-AFM structure resulting from freezing in the dominant unstable M_3^+ and/or R_4^+ oxygen octahedron rotation modes are quite small. The largest energy gain we found was 6.2 meV/f.u., for $R_4^+[001]$ rotation angle of 4.8°, resulting in a $I4/mcm$ structure. This is consistent with the experimental observation that AFM SrMnO$_3$ has a cubic structure but transforms to the $I4/mcm$ structure with a small fraction of A-site substitution by the smaller cation Ca [13]. For FM ordering, the energy of the equilibrium cubic structure is 76 meV/f.u. higher than that of the G-AFM cubic structure, and all FM structures are higher in energy than the lowest-energy AFM structure, despite the lower frequencies of the M, R and Γ modes and larger relaxation energies.

The restrictions on lattice vectors at 0% epitaxial strain change these distortions and energy differences only slightly; the results for the latter are included in Fig. 1. For example, the tetragonal relaxation of the FM state lowers its energy slightly, so that the AFM-FM splitting is 84 meV/f.u.

In Fig. 1, the epitaxial strain dependence of the total energies of various structures and magnetic orderings is shown for tensile strain from 0% to 5%. Because of their coupling to strain, the lowest frequency polar modes in the G-AFM $P4/mmm$ and $Imma(R_4^+[110])$ structures become unstable at a critical strain of about 1%, with second-order phase transitions to the polar $Amm2(\Gamma_4^-[110])$ and $Ima2(R_4^+[110] + \Gamma_4^-[110])$ phases, respectively. This epitaxial-strain-induced ferroelectricity in the antiferromagnetic state is analogous to that previously found in nonmagnetic $P4/mmm$ SrTiO$_3$ [4,5], $Pnma$ CaTiO$_3$ [6] and antiferromagnetic $Pnma$ CaMnO$_3$ [26], with critical strains of 0.6%, 2%, and 2% respectively; hypothetical antiferromagnetic cubic BaMnO$_3$ [27] is already ferroelectric at its equilibrium lattice constant. The dependence of the total energies on compressive strain, not shown, produces an analogous effect at -2.9% strain.

Here, we focus instead on the interplay of the strain and polar instability with the magnetic ordering. In contrast to the AFM phases, the energy of FM structures initially decreases with increasing tensile strains (Fig. 1); this corresponds to the slightly larger computed lattice constant for FM ordering in the undistorted cubic structure. The polar instability leads to a substantial energy lowering which increases with increasing strain, so that at tensile strains
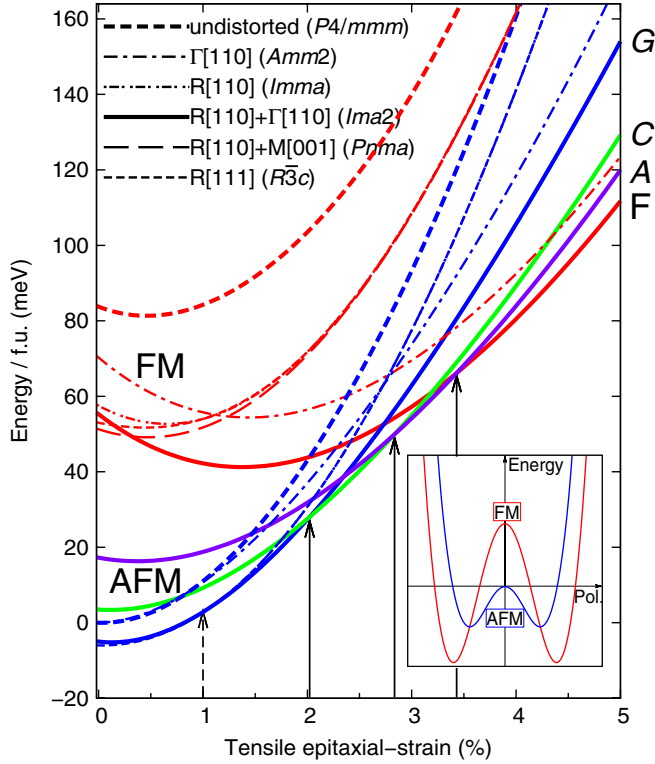
FIG. 1 (color online). $GGA + U$ total energies of various structures, per formula unit, obtained by freezing in the given mode(s). Calculations were performed at integer values of strain and interpolated. The energies of structures with FM ordering are shown in red, for G-AFM in blue, C-AFM in green and A-AFM in violet. Vertical black dotted lines at 1.0%, 2.0%, 2.8%, and 3.4% strain indicate phase boundaries separating $Imma(G$-AFM$)$, $Ima2(G$-AFM$)$, $Ima2(C$-AFM$)$, $Ima2(A$-AFM$)$, and $Ima2($FM$)$ states. The inset is a schematic showing the stability of the FM-FE state at large strain.

above 3.4% the energy of the $Ima2$ FE-FM structure drops below those of the AFM-FE phases (see inset); for compressive strains, the FE-FM structure with space group $I4cm(R_4^+[001] + \Gamma_4^-[001])$ is favored above a critical strain of -2.9%. The polar distortion with strain also drives a metal-insulator transition above a critical amplitude; at all strains considered, the FE-FM phase is insulating, with a band gap ranging from 0.22 eV at 0% strain to 0.51 eV at 5% strain.

In addition to G-AFM ordering, we also considered $R_4^+[110] + \Gamma_4^-[110]$ phases with C-AFM and A-AFM orderings, in which some fraction of nearest neighbor Mn moments are parallel. Though higher in energy than G-AFM at 0% strain, they are favored by increasing tensile strain. As can be seen in Fig. 1, the polar C-AFM phase, with 1/3 parallel-spin bonds, drops below G-AFM at 2%, and the A-AFM phase, with 2/3 parallel-spin bonds, drops below the C-AFM phase at 2.8%. For compressive strain, however, the distorted G-AFM state is lower in energy than the A and C states up to the strain where the FM state becomes lower in energy, and thus there are no intermediate transitions. We note that in all the AFM phases that

appear in the epitaxial strain phase diagram, weak ferromagnetism is allowed by symmetry. However, the moment is proportional to the spin-orbit coupling. It thus would be expected to be quite small, and is not included in the calculations presented here.

There are thus four phase transitions in the range of tensile strain considered: G-AFM $-$ PE $\rightarrow$ G-AFM $-$ FE $\rightarrow$ C-AFM $-$ FE $\rightarrow$ A-AFM $-$ FE $\rightarrow$ FM $-$ FE. The strain dependence of the electric polarization and of the estimated Néel (for AFM phases) and Curie (for the FM phase) temperatures are shown in Fig. 2. The three first-order magnetic transitions are of particular interest. At each of these, the change in magnetic order is accompanied by a change in the magnitude of the electric polarization. The magnitude of the polarization change makes typical electric energies ($PE = 10 \; \mu\text{C}/\text{cm}^2 \times 50 \; \text{kV}/\text{cm} = 0.2 \; \text{meV}/\text{f.u.}$) comparable to typical magnetic energies ($MH = 3 \; \mu_B \times 1T = 0.2 \; \text{meV}/\text{f.u.}$). Thus, near the A-AFM $-$ FE $\rightarrow$ FM $-$ FE phase boundary, an applied electric field can induce a nonzero magnetization. A substantial magnetodielectric coupling is also expected at that phase boundary as a magnetic-field-induced transition to the FM phase will also lead to a jump in the FE polarization and in the dielectric constant. At the AFM-FE/FM-FE phase boundary for compressive strain, in addition to an analogous magnetodielectric coupling, a strong strain response is expected due to the jump in c lattice parameter.

In $GGA + U$, the overestimate of the cell volume may lead to a spurious enhancement of the polar instability. We have investigated this effect by performing calculations for the four lowest-energy phases with LSDA $+ U$, where the underestimate of the volume is expected to lead to a comparable suppression of the polar instability. As can be seen from the linear phase diagram at the top of Fig. 2, epitaxial-strain-induced ferroelectricity in the G-AFM phase moves to larger strain, and the relative stability of the C-AFM and A-AFM phases decreases, so that the transition from G-AFM-FE to FM-FE occurs at a higher critical strain of 5.5%, which can be regarded as an upper bound. We thus estimate the critical strains for the FM-FE phase to be $+4.5 \pm 1\%$ (tensile strain), and $-4.9 \pm 2\%$ (compressive strain).

It is well known that changes in the choice of the parameter U can have a significant effect on magnetic ordering energies; this was shown, in particular, in EuTiO$_3$ [7]. We have verified that the epitaxial-strain-induced multiferroicity occurs for a wide range of possible choices of U, though the quantitative details change.

The critical strain for observation of the FM-FE phase in SrMnO$_3$ is rather high, which may make experimental confirmation challenging. Observation of the behavior characteristic of lower strains, such as the strain-induced ferroelectricity in G-AFM and the decrease in T_N in the G-AFM PE and FE phases, should be taken as indicators of the impending transition to the FM-FE phase at higher strain.
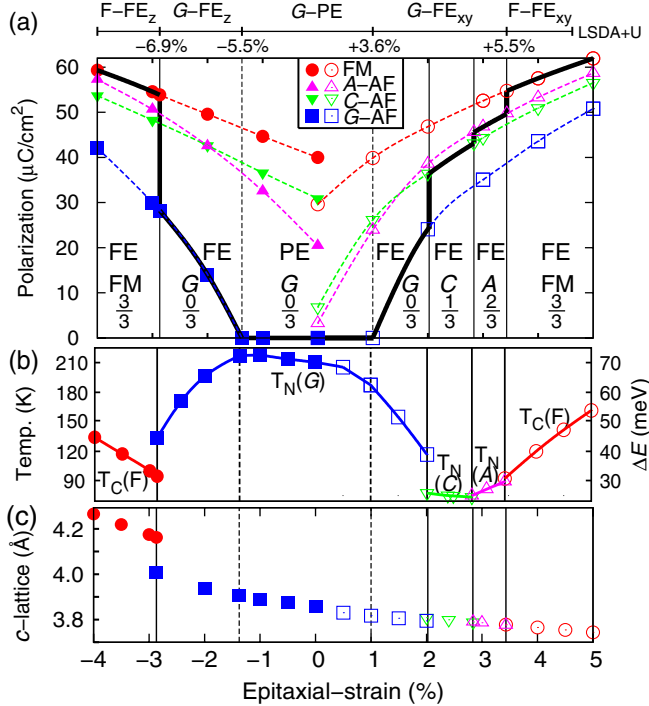
FIG. 2 (color online).   (a) Computed ferroelectric polarization of SrMnO$_3$ G-AFM (square), C-AFM (down triangle), A-AFM (up triangle) and FM (circle) in the lowest energy structure at each strain value. The fractions of parallel nearest neighbor spins in each state are given. The bold black line follows the polarization of the lowest energy structure with changing strain. The linear phase diagram at the top, not on the same scale, shows the phases and phase boundaries as computed within LSDA + U for comparison. Open and solid symbols represent structures where R rotation is along [110] and [001], respectively. (b) Magnetic ordering temperatures were estimated from computed values of ΔE as described in the text. (c) c lattice parameter for the lowest energy structure at each strain value.

In summary, we have presented first-principles calculations that reveal a large spin-phonon coupling in cubic SrMnO$_3$. Through combination of this coupling with the polarization-strain coupling characteristic of perovskite oxides, both tensile and compressive epitaxial strain drive the system through a series of phase transitions to a ferromagnetic-ferroelectric multiferroic state. As the magnetic transitions are accompanied by a jump in electric polarization, there is the possibility of electric field control of magnetic ordering; at the two boundaries between AFM and FM phases, the polarization can conversely be controlled by an applied magnetic field. At this boundary for compressive strain, the jump in c lattice parameter also should yield a strong strain response to applied fields. Though the cubic FM phase is metallic, the polar distortion opens a gap in the electronic density of states, resulting in the insulating character of the FM-FE phase. This suggests that the search for epitaxial-strain-induced multiferroics

could be productively extended to include other systems with metallic character for the FM reference state.

*jhlee@physics.rutgers.edu

[1] N. A. Spaldin and M. Fiebig, Science **309**, 391 (2005).
[2] R. Ramesh and N. A. Spaldin, Nature Mater. **6**, 21 (2007).
[3] S. W. Cheong and M. Mostovoy, Nature Mater. **6**, 13 (2007).
[4] J. H. Haeni et al., Nature (London) **430**, 758 (2004).
[5] A. Antons, J. B. Neaton, K. M. Rabe, and D. H. Vanderbilt, Phys. Rev. B **71**, 024102 (2005).
[6] C.-J. Eklund, C. J. Fennie, and K. M. Rabe, Phys. Rev. B **79**, 220101(R) (2009).
[7] C. J. Fennie and K. M. Rabe, Phys. Rev. Lett. **97**, 267602 (2006); (to be published).
[8] T. Katsufuji and H. Takagi, Phys. Rev. B **64**, 054415 (2001).
[9] A. P. Ramirez, J. Phys. Condens. Matter **9**, 8171 (1997).
[10] A. Asamitsu, Y. Moritomo, Y. Tomioka, T. Arima, and Y. Tokura, Nature (London) **373**, 407 (1995).
[11] N. Ray and U. V. Waghmare, Phys. Rev. B **77**, 134112 (2008).
[12] J. H. Lee and K. M. Rabe (to be published).
[13] O. Chmaissem et al., Phys. Rev. B **64**, 134412 (2001).
[14] T. Takeda and S. Ohara, J. Phys. Soc. Jpn. **37**, 275 (1974).
[15] C. Loschen, J. Carrasco, K. M. Neyman, and F. Illas, Phys. Rev. B **75**, 035115 (2007).
[16] J. P. Perdew, K. Burke, and M. Ernzerhof, Phys. Rev. Lett. **77**, 3865 (1996).
[17] G. Kresse and J. Hafner, Phys. Rev. B **47**, R558 (1993).
[18] G. Kresse and J. Furthmüller, Phys. Rev. B **54**, 11 169 (1996).
[19] S. L. Dudarev, G. A. Botton, S. Y. Savrasov, C. J. Humphreys, and A. P. Sutton, Phys. Rev. B **57**, 1505 (1998).
[20] S. Picozzi et al., Phys. Rev. B **75**, 094418 (2007).
[21] P. E. Blöchl, Phys. Rev. B **50**, 17 953 (1994); G. Kresse and D. Joubert, Phys. Rev. B **59**, 1758 (1999).
[22] N. A. Pertsev, A. G. Zembilgotov, and A. K. Tagantsev, Phys. Rev. Lett. **80**, 1988 (1998).
[23] O. Diéguez et al., Phys. Rev. B **72**, 144101 (2005).
[24] R. D. King-Smith and D. Vanderbilt, Phys. Rev. B **47**, 1651 (1993).
[25] J. Samuel Smart, Effective Field Theories of Magnetism (Saunders Company, Philadelphia, 1966).
[26] S. Bhattacharjee, E. Bousquet, and Ph. Ghosez, Phys. Rev. Lett. **102**, 117602 (2009).
[27] J. M. Rondinelli, A. S. Eidelson, and N. A. Spaldin, Phys. Rev. B **79**, 205119 (2009).